1 Channel evolution processes in a diamictic glacier foreland. Implica-
2 tions on downstream sediment supply: case study Pasterze / Austria

3 Michael Paster[1], Peter Flödl[1], Anton Neureiter[2], Gernot Weyss[2], Bernhard Hynek[2], Ulrich Pulg[3],
4 Rannveig Ø. Skoglund[4], Helmut Habersack[1], Christoph Hauer[1]

5 [1]CD-Laboratory for Sediment research and management, Institute of Hydraulic Engineering and River Research, Department
6 of Water, Atmosphere and Environment, University of Natural Resources and Life Sciences Vienna, Muthgasse 107, 1190
7 Vienna, Austria
8 [2]Department for Climate Research, Central Institute for Meteorology and Geodynamics, Hohe Warte 38, 1190 Vienna, Austria
9 [3]UNI Research Miljø, Laboratorium for Freshwater Ecology and Inland Fisheries, Nygårdsgaten 112, 5006 Bergen, Norway
10 [4]University of Bergen, Fosswinckelsgt. 6, 5006, Bergen, Norway

11 *Correspondence to*: *Michael Paster (michael.paster@boku.ac.at)*

12 **Abstract.** Global warming and glacier retreat are affecting the morphodynamics of proglacial rivers. In response to changing
13 hydrology, their altered hydraulics will significantly impact future glacifluvial erosion and proglacial channel development.
14 This study analysis proglacial channel evolution processes at the foreland of Austria's biggest glacier Pasterze by predicted
15 runoff until 2050. A high-resolution digital elevation model was created by an unmanned aerial vehicle, channel bathymetry
16 was sampled, a one-dimensional hydrodynamic-numerical model was generated, and bedload transport formulas were used to
17 calculate the predicted transport capacity of the proglacial river. Due to the fine sediment composition near the glacier terminus
18 (d_{50}< 49.6 mm), the calculation results underline the process of headward erosion in the still unaffected, recently deglaciated
19 river section. In contrast, an armor layer is already partly established by the coarse grain size distribution in the already incised
20 river section (d_{50}> 201 mm). Furthermore, already reoccurring exposed non-fluvial grain sizes combined with decreasing flow
21 competence in the long term are indicators for erosion-resistant pavement layer formation and landform decoupling in the
22 vertical direction. The presented study clearly shows that subsystems of 'developed channels' exhibiting pavement formation
23 of non-fluvial deposits are found at the investigated glacier foreland. Thus, an extension accompanied by a refinement of the
24 fluvial system in the sediment cascade approach was developed as a central result.

25 1 Introduction

26 Since the Little Ice Age (LIA) around 1850, global warming has caused temporal and spatial changes in high mountain areas
27 by glacier retreat (e.g., Zemp et al., 2019; Fischer et al., 2018; Huss et al., 2008) and permafrost decline (Harris et al., 2009).
28 While deglaciation of European glaciers has accelerated and repeatedly reached peak values in recent years (Sommer et al.,
29 2020), formerly glaciated areas are continuously expanding and are characterized by high geomorphological activity (e.g.,
30 Avian et al., 2018; Lane et al., 2016; Carrivick et al., 2013; Cavalli et al., 2013; Old et al., 2005; Gruber et al., 2004).

Hydrology and
Earth System
Sciences
Discussions

31   Deglaciated areas in direct proximity to the glacier terminus are termed proglacial (Slaymaker, 2009) and are confined by LIA
32   moraines (Heckmann & Morche, 2019). Within this steadily increasing spatial boundary, the amount of loose and
33   unconsolidated sediment exceeds the 'geological norm' defined by non-glaciated catchments. Proglacial areas are, therefore,
34   transitional landscapes that adapt to this geological norm within the paraglacial period (Ballantyne, 2002; Church & Ryder,
35   1972). This adjustment occurs by various geomorphological processes (e.g., gully erosion, avalanches, debris flows), where
36   sediment is reworked along the gravitational gradient (Ballantyne, 2002). In contrast, continuous sediment supply is given by
37   (sub)glacial erosion (e.g., Hallet et al., 1996; Alley et al., 2019) and moderately well-rounded (Benn & Evans, 2013) poorly
38   sorted unconsolidated material ranging in size from sand to cobbles up to boulders (diamictic till; Harland et al., 1966) is
39   deposited in the outwash plain by meltwater (Benn & Evans, 2013). The sediment production and reworking process chain of
40   (temporary) sediment storages within a catchment can be described by the 'sediment cascade approach' (Chorley & Kennedy,
41   1971). The sediment connectivity between these storage landforms in longitudinal (in-stream linkage), lateral (e.g., channel –
42   hillslope relationship), and vertical (channel bed – subsurface connection) direction (Fryris et al., 2007) is highly dynamic
43   (Lane et al., 2016) and crucial if sediment from different origins reaches the valley floor and contributes to the glacifluvial
44   transport in the proglacial channel network (e.g., Beylich et al., 2019; Brierley et al., 2006). Fluvial sediment evacuation is
45   considered as the last transport process of the sediment cascade (e.g., Geilhausen et al., 2012b; Etzelmüller & Frauenfelder,
46   2009; Schrott et al., 2003; Chorley & Kennedy, 1971) and is predominant in the paraglacial period (Church & Ryder, 1972).
47   Alpine proglacial areas are in general highly dynamic fluvial systems (e.g., Leggat et al., 2015; Micheletti et al., 2015; Mao et
48   al., 2014; Gurnell, 1995; Warburton, 1992), triggered by daily to seasonal meltwater fluctuations and high-magnitude/low-
49   frequency events (e.g., Baewert & Morche, 2014; Marren, 2005; Beylich & Gintz, 2004). Combined with the high sediment
50   supply by erosion of glacifluvial diamictic till, braided channels emerge in direct glacier proximity (e.g., Maizels, 2002;
51   Gurnell et al., 1999; Ashworth & Ferguson, 1986). More downstream with increasing distance to the glacier terminus,
52   depending on (i) sediment composition, (ii) runoff variability, (iii) channel slope, and (iv) potential confinement (e.g.,
53   moraines, glacier ice), the channel turns into a single thread river (e.g., Marren, 2005; Gurnell et al., 1999). Another dominant
54   process supporting the formation of single channels, however, is river bed incision when the transport capacity exceeds the
55   sediment supply (e.g., Wilkie & Clague, 2009; Marren, 2005; Gurnell et al., 1999). This kind of glacifluvial process leads to
56   the exposure of non-fluvial sediment in formerly glaciated environments and creates an armor layer (Bunte & Abt, 2001).
57   Fluvial sediment transport, which mainly contributes to the stabilization of proglacial areas, especially with increasing distance
58   to the glacier terminus (e.g., Delaney et al., 2018; Lane et al., 2016), is described in the sediment cascade as a glacifluvial
59   process (Geilhausen et al., 2012b). Whether this process is able for sediment transport or sediment remains deposited is defined
60   by the hydraulic parameter 'flow competence' – defined as the largest particle a flow can move (Benn & Evans, 2013).
61   Flow competence is mainly impacted by the runoff conditions, which are predicted to change by global warming (e.g., Förster
62   et al., 2015; Farinotti et al., 2012; Braun et al., 2000). The glacier mass of the Austrian Alps is expected to decrease
63   continuously (Fischer et al., 2018), which implies changes in the future glacial discharge regimes: (i) on a short time scale,
64   glacial meltwater will increase due to deglaciation, (ii) in a long-term perspective, the runoff will decrease by 'exceeding the

Hydrology and
Earth System
Sciences
Discussions

65 expected moment of peak water' (Schaefli, 2015; Farinotti et al., 2012). This exceedance is predicted before 2050 for European

66 glaciers (Huss & Hock, 2018); after that, the runoff will lose its glacial characteristic over time. Alongside these predictions,

67 (i) the annual peak runoff will be shifted to spring (Förster et al., 2015), and (ii) reduced average peak runoff will hence the

68 bedload transport of proglacial rivers (Pralong et al., 2015). All these predictions mainly affect the flow competence of rivers

69 and impact channel bed stabilization by glacifluvial erosion, the last process of proglacial sediment cascade models.

70 This study aims to predict the effect of global warming on proglacial channel evolution. For this purpose, the proglacial part

71 of the river Möll at the foreland of Austria's biggest glacier Pasterze was investigated. Currently, the sediment yield of the

72 Pasterze catchment consists mainly of suspended sediment (Avian et al., 2018; Geilhausen et al., 2012b). Whether this behavior

73 remains the same in the future by changing runoff characteristics was investigated using predicted runoff by 2050. A high-

74 resolution digital elevation model (DEM) was created for hydrodynamic numerical modeling, and bedload transport formulas

75 were used to predict the proglacial channel's flow competence. The ongoing establishment of a pavement layer by (exposed)

76 non-fluvial sediment in sections with greater distance to the glacier forces a landform decoupling. The results obtained allow

77 a revision and extension of the fluvial system of the sediment cascade approach by incorporating the effects of global warming.

2 Study site

79 The investigation area is located in Carinthia in the national park Hohe Tauern at the foreland of the Pasterze Glacier

80 (47°5'8" N; 12°42'27" E), the biggest glacier in Austria and the Eastern Alps (16.2 km² in 2012). The glacier tongue (~4 km

81 length) is characterized by (i) a high mean annual rate of retreat of up to -50 ma^{-1} (Fischer et al., 2018) and (ii) a debris coverage

82 of around 75 % (Kellerer-Pirklbauer, 2008). The total length loss of the Pasterze Glacier since LIA amounts to -2200 m until

83 2015 (Fischer et al., 2018). The debris mantle at the southern part (orographic right) of the glacier tongue results in a lower

84 deglaciation rate of up to 35 % by a minimum debris thickness of 15 cm (Kellerer-Pirklbauer et al., 2008). The proximal glacier

85 foreland is characterized by a low gradient (Geilhausen et al., 2012b; Krainer & Poscher, 1992), debris-covered dead ice

86 landforms (e.g., Avian et al., 2018; Seier et al., 2017; Geilhausen et al., 2012a) and one main proglacial river.

2.1 Proglacial river

88 The investigated reach covers around 850 m between the glacier terminus (2100 m a.s.l.) and the inflow (delta area) into the

89 continuously increasing lake 'Pasterzensee' (upstream of the lake "Sandersee", which formed in the late 1950s; Krainer &

90 Poscher, 1992) at 2070 m a.s.l. (Fig. 1). The channel is composed of four distinct sections: (i) the flat headwater near the

91 glacier terminus (L= 200 m; S_m= 1.3 %), (ii) a transition section (L= 100 m; S_m= 2.9 %) into (iii) the canyon (L= 482 m; S_m=

92 6.8 %), and (iv) the flat outlet into the delta area (L= 60 m; S_m= 1.7 %) of the lake 'Pasterzensee'. Almost the entire investigated

93 proglacial channel (except the delta area) is confined by the debris-covered glacier tongue and debris-covered dead ice (with

94 slower melting rates). The runoff behavior shows typical glacial characteristics with (i) high summer (up to Q_{max}= 25 m³s^{-1})

95 and low winter runoff (down to Q_{min}= 0.1 m³s^{-1}) and (ii) strong seasonal and diurnal fluctuations (Krainer & Poscher, 1992).
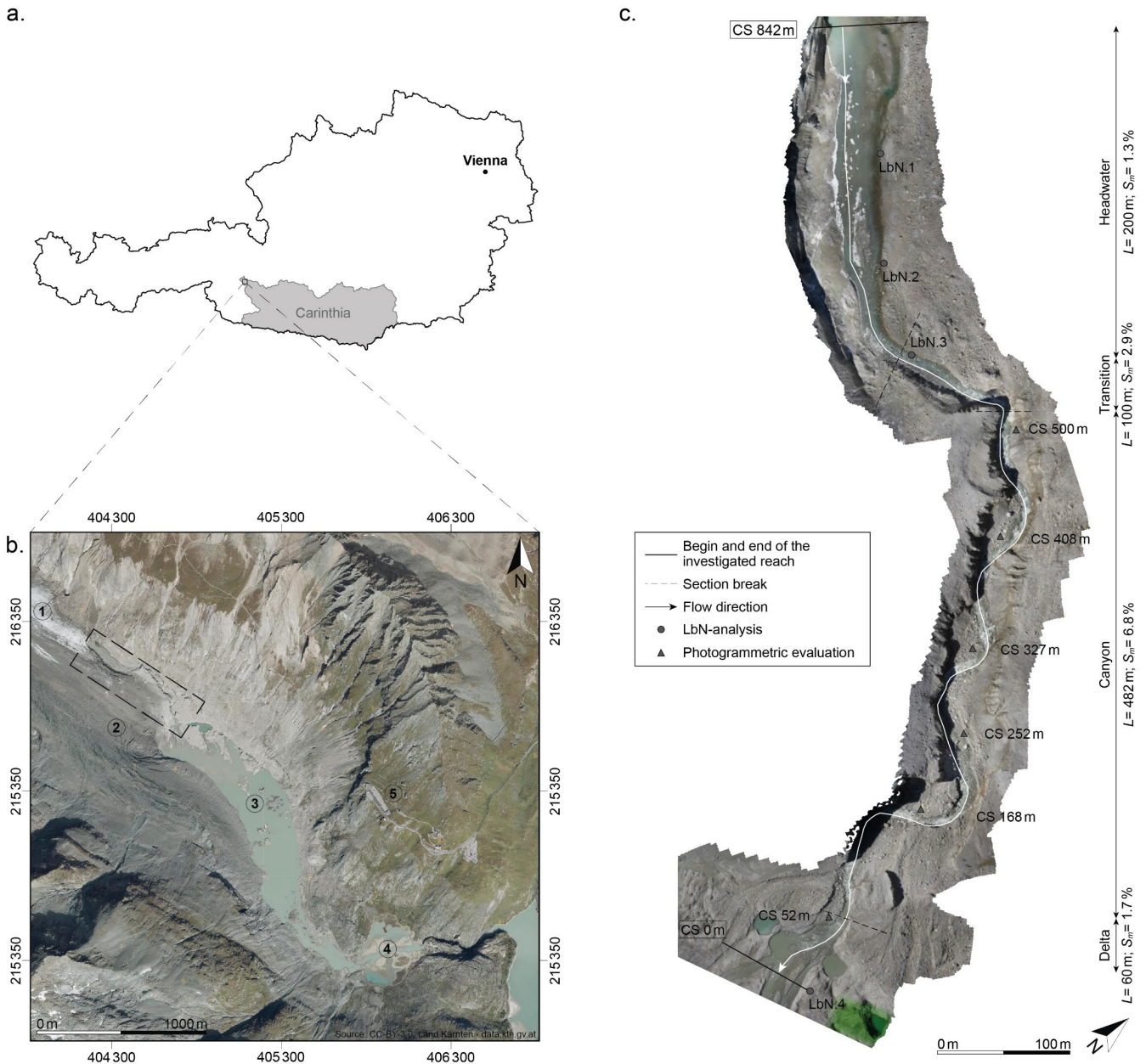
Figure 1: Location of the study site: **(a.)** Carinthia, Austria; **(b.)** proximal foreland of the Pasterze Glacier, where the dashed rectangle indicates the proglacial river Möll including *(1)* glacier tongue (clean), *(2)* glacier tongue (debris-covered), *(3)* Pasterzensee, *(4)* Sandersee, *(5)* Kaiser-Franz-Josefs-Höhe; **(c.)** study reach, based on the own UAV survey, supplemented by the measuring sites for sediment analysis.

2.2 Sediment budget

The proximal foreland of the Pasterze Glacier is characterized by glacifluvial deposits, including big boulders, gravel, and sand (Fig. 2), which partly cover dead ice landforms (e.g., Avian et al., 2018; Seier et al., 2017; Geilhausen et al., 2012a). This moderately well-rounded, poorly sorted outwash (glacial diamictic till; Harland et al., 1966) is decoupled from the active

104 hillslopes around the proximal foreland, resulting in a transport-limited glacifluvial transport system (Geilhausen et al., 2012b).

105 The potential for paraglacial reworking on the overall sediment output is low compared to glacifluvial processes, especially

106 with increasing distance to the glacier terminus (Geilhausen et al., 2012a; 2012b). However, this proglacial area is still a

107 dynamic system with a high potential for fluvial reworking processes (Avian et al., 2018). The biggest proportion of the

108 sediment output is assumed as suspended load (Geilhausen et al., 2012b).

110 **Figure 2:** River embankment of the investigated proglacial canyon already incised in the poorly sorted diamictic outwash plain (photographs
111 taken during fieldwork).

3 Methods

3.1 UAV survey

114 The mapping was carried out during low flow conditions in autumn 2018, where the 850 m long river stretch (Fig. 1) was

115 covered by an unmanned aerial vehicle (UAV; type: hexacopter KR 615) equipped with a compact camera (type: Sony ILCE-

116 6000; focus length 16 mm) mounted on a stabilized gimbal. The survey was performed in two stages: (i) the entire study area

117 was covered with a constant flight level of 55 m above the river bed and (ii) the canyon in a second flight with a constant flight

118 level of 20 m above the channel bed (approx. surrounding terrain level). In total, 1371 photos (6000x4000 px) were taken,

119 whereby a requested overlap of 80 % (forward) and 60 % (sideward) was achieved. Before the flights, ground control points

120 (GCPs) were placed along the banklines to improve the geodetic accuracy of the digital elevation model (DEM). Due to limited

121 accessibility and high and steep channel embankments, no GCPs were laid out in the channel. All GCPs were mapped by an

122 RTK-enabled GNSS device (type: Emlid Reach RS2).

3.2 DEM preparation

In post-processing, the software PhotoScan by Agisoft was applied to create (i) a 3D point cloud and (ii) an orthomosaic according to the principle of Structure-from-Motion (SfM). This approach uses images taken from multiple perspectives to compute a 3D surface based on image-matching algorithms combined with multi-view stereo techniques (MSV). This process allows the calculation of the camera position and orientation (Snavely et al., 2008). The mapped GCPs were used for geo-referencing the model and accuracy assessment of the transformation (Fonstad et al., 2013).

First, 1371 photos were used in the alignment, the camera position and the orientation of the individual photos were estimated, and a sparse point cloud with 365 080 points was calculated. The mapped coordinates of 10 GCPs were assigned for geo-referencing in the next step. The sparse point cloud was purged to (i) remove high outliers and misaligned points (down to 295 371 points), (ii) optimize the camera position, and (iii) minimize the error between the GCPs. This refinement, including the accuracy assessment by the remaining four GCPs, led to a root-mean-square error (RMSE) of 0.056 m (X_{RMSE}= 0.025 m; Y_{RMSE}= 0.044 m; Z_{RMSE}= 0.024 m). In the third step, the DEM was calculated (478 231 187 points; 3940 points m^{-2}) with a ground sample distance (GSD) of 1.59 cm px^{-1}, and an orthomosaic was arranged.

3.3 Sediment sampling

The sediment sampling was done by the commonly used method for gravel to cobble-bed mountain rivers according to Fehr (1987). For the accessible river sections, the line-by-number method (LbN) was applied, where all grains (b-axis) along the projection of a line are sampled and measured (at least 150 stones). Four LbN-analyses at characteristic points were carried out and mapped with the RTK GNSS device (circles in Fig. 1). For the inaccessible canyon, sediment analysis was photogrammetrically in post-processing on the images taken during the UAV mapping. At six characteristic points (triangles in Fig. 1), the grains were measured manually according to the on-site method by Fehr (1987). Both applied methods only take the coarse fractions into account (partially grain size distribution), which was sufficiently accurate for the objectives of this study: while Fehr (1987) suggests the cut-off at $b \geq 1$ cm, the truncation for adequate identification of grains in the digital method is strongly dependent on the GSD ranging between $b > 10\text{-}15$ px (Detert et al., 2018) and $b > 4$ px (Lang et al., 2021).

3.4 Hydraulic Modeling

A one-dimensional hydrodynamic-numerical (HN) model was set up (using the software Hec-Ras by the United States Army Corps of Engineers) for calculating the hydraulic parameters (i) bed shear stress and (ii) energy gradient, both relevant for the used bedload transport formulas. For this objective, cross-sections (CS) at a 10 m maximum distance were generated from the high-resolution DEM. The point density was reduced (down to 490 points per CS) by applying the automatic point filter algorithm with minimum area change. The modeling was performed with steady runoff conditions and the predicted maximum mean monthly runoff until 2050 ($Q_{m.max}$), which was determined by the 'Glacier Runoff Evolution Model (GERM)' (Schöner

Hydrology and
Earth System
Sciences
Discussions

Open Access

EGU

153   et al., 2013). The inaccessibility necessitated a sensitivity analysis for roughness determination by varying representative

154   roughness values (Strickler coefficient k_{st}), which resulted in k_{st}= 28 m$^{1/3}$s^{-1} (headwater and delta) and k_{st}= 20 m$^{1/3}$s^{-1} (canyon).

3.5 Initiation of motion

156   The calculation for the initiation of motion was done by the bedload transport formula for steep mountain channels according

157   to Eq. (1) by Rickenmann (1990). To consider the increased flow resistance due to large roughness elements in the canyon,

158   the energy gradient was reduced according to Eq. (2) by Rickenmann et al. (2006).

159    $$q_c = 0.065 * \left(\frac{\rho_s}{\rho_w} - 1\right)^{1.67} * g^{0.5} * I_R^{-1.12} * d_{50}^{1.5} \tag{1}$$

160   Here, the specific discharge (q_c) is a function of the characteristic grain diameter (d_{50}), the energy gradient (I_R), and the ratio

161   between sediment (ρ_s) and fluid density (ρ_w). The calculation results according to this 'conventional approach' in this study

162   are termed $d_{50.c}$.

163    $$I_{red} = I_R * \left[\frac{n_r}{n_{tot}}\right]^a \tag{2}$$

164   Here, the reduced energy gradient (I_{red}) is calculated by the ratio of the grain roughness (n_r) and total roughness (n_{tot}), a= 1.5

165   is a constant. The calculation results with the reduced energy gradient are labeled with $d_{50.r}$ in this study.

166   The characteristic grain size d_{90}, required for this calculation step, was derived from the adjusted Wolman count method for

167   the entire canyon, as Hauer & Pulg (2018) described. According to this field-based method, the assumed b-axis of the three

168   largest stones were manually measured in each cross-section of the canyon on the high-resolution UAV aerial images. In total,

169   159 stones were measured (b= 546-3715 mm), which resulted in a mean d_{90}= 1290 mm for the entire canyon.

3.6 Determination of morphological changes

171   Due to the lack of multitemporal terrain data, a comparative analysis based on an orthophoto of 2015 was performed to

172   reconstruct the evolution of the proglacial channel (formed in the ablation season of 2015). The channel formation was verified

173   by continuously recorded images from an automatic camera installed at the Kaiser-Franz-Josefs-Höhe (Fig. 1). Due to the

174   recording rate of 5 minutes, the proglacial area can be observed in a high temporal resolution (compare Avian et al., 2020).

4 Results

4.1 Sediment analysis

177   The results for all ten grain size distribution curves can be described as narrowly graded, reflected in a very steep gradient of

178   each curve (Fig. 3a). The sediment composition in the direction of flow is becoming increasingly coarse $(d_{50.m:LbN.1}$= 29.9 mm

179    $< d_{50.m:LbN.2}$= 49.6 mm $< d_{50.m:LbN.3}$= 79.6 mm) with the same distribution in the delta area $(d_{50.m::LbN.4}$= 40.3 mm) as in the

180   headwater. The evaluation of the UAV-based sediment measurements (six characteristic points in the canyon; triangles in Fig.

Hydrology and
Earth System
Sciences
Discussions

Open Access
EGU

181   1) illustrate a much coarser composition $(d_{50.m:CS500}=$ 202.5 mm; $d_{50.m:CS408}=$ 219.1 mm; $d_{50.m:CS327}=$ 241.2 mm; $d_{50.m:CS252}=$

182   201.3 mm; $d_{50.m:CS168}=$ 211 mm; $d_{50.m:CS52}=$ 116.3 mm). Large particles were measured in every characteristic point (up to $d_{90.m}$

183   = 850 mm), and the largest grain size was detected in the steepest part of the entire proglacial channel (b= 3700 mm).
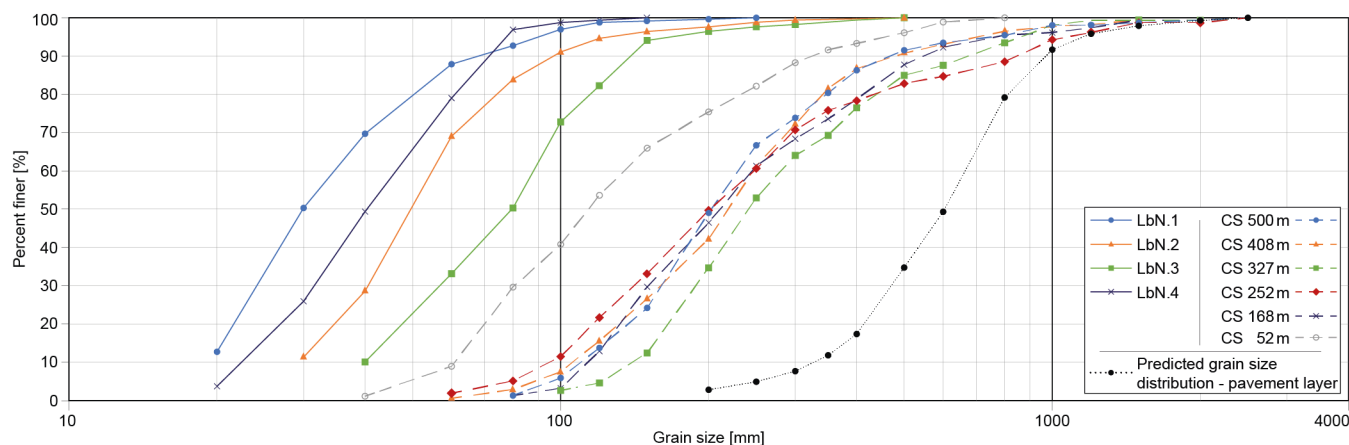
184
185   **Figure 3:** Partial grain size distribution curves: **(a.)** four line-by-number (LbN) analyses (continuous lines) and photogrammetric evaluations
186   (dashed lines) for six characteristic points in the inaccessible canyon. **(b.)** the dotted black curve refers to the potential future grain size
187   distribution of the pavement layer.

188   **4.2 Development of flow competence**

189   The seasonal course of the flow competence (the largest particle a flow can move) runs parallel to the typical glacial discharge

190   regime: smaller transportable grain sizes in the cold months and largest transportable grain sizes in the ablation season (summer

191   months). According to the forecasted hydrograph, the maximum mean monthly runoff $(Q_{m.max})$ will continuously increase in

192   the ablation seasons until June 2030 $(Q_{m.max.2030}=$ 14.61 m³s⁻¹), following a decrease until 2050 $(Q_{m.max.2015}=$ 12.74 m³s⁻¹), which

193   will be again around the level of 2018 $(Q_{m.max.2018}=$ 12.19 m³s⁻¹). Crucial for this runoff development may be the exceedance

194   of the expected moment of peak water after 2030, where the maximum mean monthly meltwater runoff $(Q_{m.melt.max})$ is predicted

195   to decrease by two orders of magnitude until 2050 $(Q_{m.melt.max.2030}=$ 7.03 m³s⁻¹ $>>$ $Q_{m.melt.max.2050}=$ 3.50 m³s⁻¹).

196   A detailed consideration of the calculated flow competence (characteristic grain sizes $d_{50.c}$; $d_{50.r}$) according to $Q_{m.2030}$ and the

197   grain size measurements $(d_{50.m})$ in the longitudinal course shows two contrary results between (i) the flat headwater and (ii)

198   the canyon. The maximum calculated characteristic grain sizes near the glacier terminus (CS 842 m – CS 600 m; $S_m=$ 1.3 %;

199   no big roughness elements; Fig. 1) by the conventional approach according to Rickenmann (1990) are bigger than those

200   determined on-site by the LbN-analysis (up to $d_{50.c}=$ 59.4 mm $>$ $d_{50.m}=$ 49.6 mm; Fig. 4a). In the transition section (CS 650 m

201   – CS 550 m) with a slightly increased channel gradient $(S_m=$ 2.9 %), a much bigger characteristic grain size was calculated

202   then measured $(d_{50.c}=$ 275.5 mm $>$ $d_{50.m}=$ 79.6 mm). For the flow competence in the steep canyon (CS 550 m – CS 62 m; $S_m=$

203   6.8 %; big roughness elements), the opposite was observed, as the calculated characteristic grain size with the reduced energy

204   gradient (I_{red}) is smaller than measured in the aerial images (up to $d_{50.r}=$ 220 mm $<$ $d_{50.m}=$ 241.2 mm; Fig. 4b). The beginning

205   of the canyon is defined by the steepest part of the entire proglacial channel (around CS 512 m; $S_{max}=$ 18.9 %), where a so-

206 called knickpoint developed resulting in the largest calculated characteristic grain sizes ($d_{50.r}$= 320 mm). The calculation results

207 indicate for all characteristic points in the canyon that the measured characteristic grain sizes ($d_{50.m}$) theoretically exceed the

208 calculated flow competence ($d_{50.r}$) by order of 1.1-1.6 at the maximum predicted discharge ($Q_{m.max.2030}$) in June 2030 (Fig. 4).

209
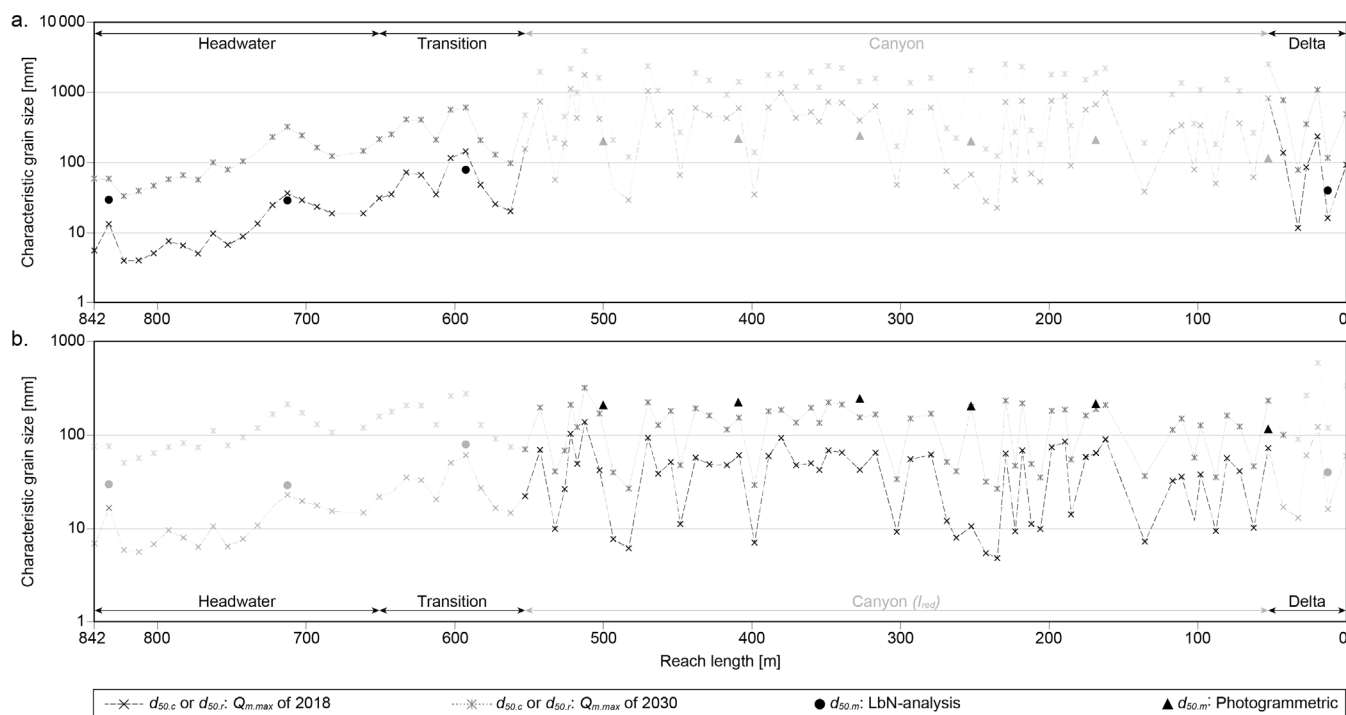
Figure 4: Longitudinal course of the calculated characteristic grain sizes (flow competence) according to **(a.)** Rickenmann (1990) ($d_{50.c}$) and
(b.) Rickenmann et al. (2006) with the reduced energy gradient ($d_{50.r}$). The transparently displayed parts of the graphs are outside the scope
of the respective approach and invalid for the respective sections. Each graph is supplemented by the measured characteristic grain sizes
($d_{50.m}$) on-site (circle) and those evaluated photogrammetrically in post-processing (triangle). The results refer to the maximum predicted
mean monthly runoff by 2050 in June 2030 ($Q_{m.max.2030}$) compared to 2018 ($Q_{m.max.2018}$).

4.3 Past morphological alterations

216 The comparison with the orthophoto of 2015 (the most recent orthophoto before the fieldwork started) shows the steepest part

217 in 2018 (around CS 512 m, S_{max}= 18.9 %) at the glacier terminus in 2015. The onset of the canyon formation in the ablation

218 season of 2015 was verified by images from the automatic camera (Fig. 5a) installed at the 'Kaiser-Franz-Josefs-Höhe' (Fig.

219 1). While no fluvial channel is visible in the ablation season of 2014, a pronounced river structure can be detected one year

220 later (August 2015; Fig. 5a). The automatically recorded images indicate a very stable canyon and a highly dynamic delta area

221 since its development. The channel pattern in this fluvial deposition zone can change annually between braided (in 2016) and

222 single thread (in 2017). Due to the confinement by the debris-covered dead ice landforms and their slower melting rate, the

223 lateral changes (ΔB) in the canyon remained largely constant except (i) at the beginning of the canyon (B= +20 m) and (ii) in

224 the most downstream part (B= +15 m; Fig. 5b) as this part was still glaciated in 2015.

Hydrology and
Earth System
Sciences
Discussions

Open Access
EGU
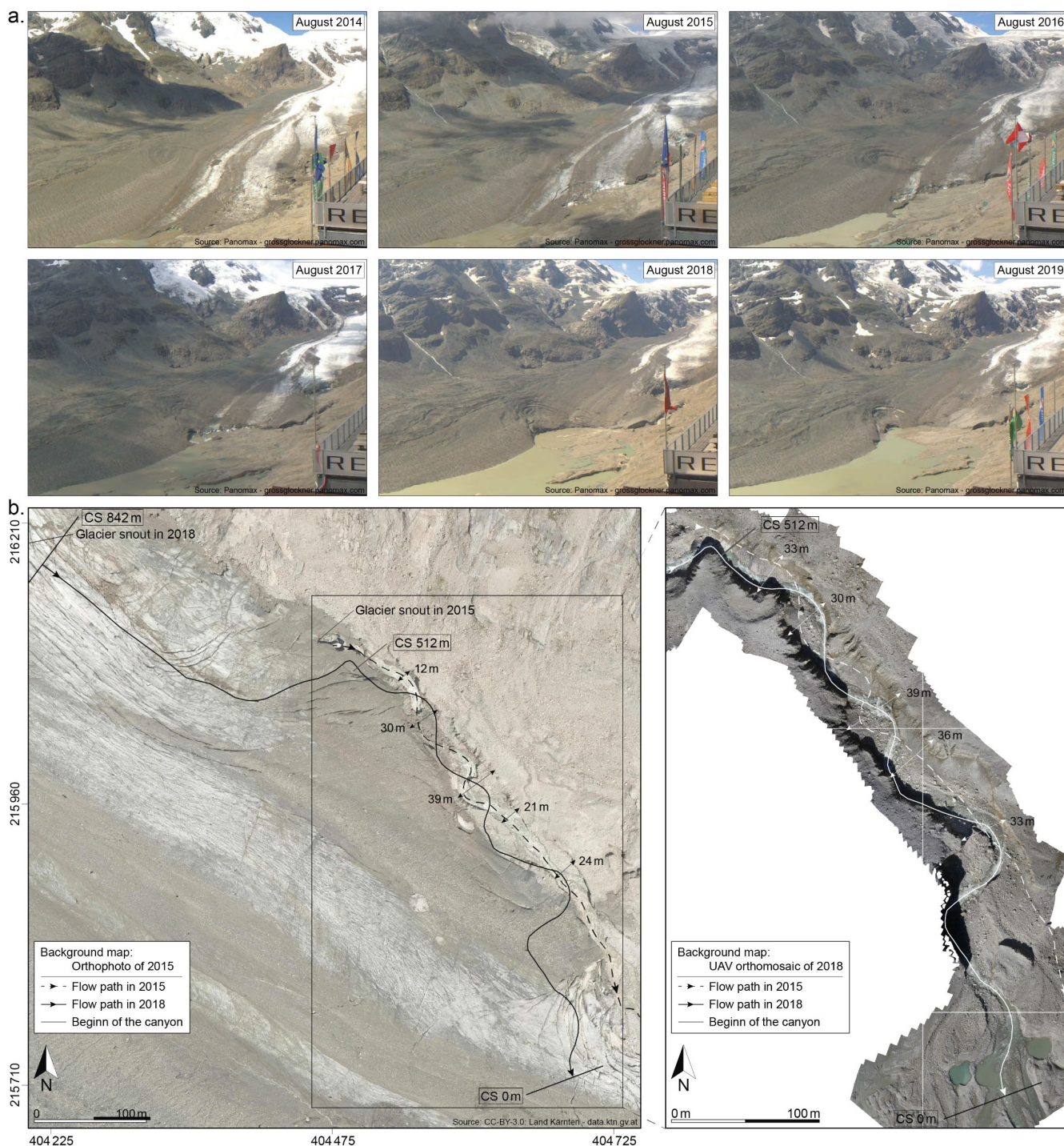
Figure 5: Proglacial fluvial channel: **(a.)** annual development stages between 2014 and 2019 recorded by the automatic camera (images provided by Großglockner Hochalpenstraße); **(b.)** comparison of flow paths after the channel formation in 2015 (orthophoto) and in the orthomosaic of 2018 (created from the own UAV survey).

Hydrology and
Earth System
Sciences
Discussions

5 Discussion

5.1 Channel evolution process

231 Channel bed incision as a stabilization process (e.g., Wilkie & Clague, 2009; Marren, 2005; Gurnell et al., 1999) was confirmed

232 in this study, but with a remarkable longitudinal differentiation. Separated by a knickpoint (e.g., Hilgendorf et al., 2020;

233 Schlunegger & Schneider, 2005), the headwater in direct glacier proximity is transitioning to the incised canyon (Fig. 6). This

234 knickpoint is defined by the highest gradient (S_{max}=18.9 %) of the entire investigated proglacial reach established by the glacier

235 terminus in 2015 (Fig. 5). The analysis of the river bathymetry and the results by the hydrodynamic model show potential for

236 river bed incision in the headwater and tendencies for stabilization processes in the canyon (Fig. 6).

237 Moreover, the shift and alteration of the runoff will cause limitations in the bedload transport (e.g., Pralong et al., 2015;

238 Geilhauesen et al., 2012b) and channel stabilization tendencies by glacifluvial sediment reworking are given with increasing

239 distance to the glacier terminus (e.g., Delaney et al., 2018; Lane et al., 2016; Gurnell et al., 1999). The dominant process in

240 the headwater is headward erosion, already known from, e.g., a fluvial drainage basin in Switzerland (Schlunegger &

241 Schneider, 2005). Starting from this point with the highest gradient *(S_{max})*, the glacifluvial erosion will shift the knickpoint

242 more upstream (Hilgendorf et al., 2020). The first indicators of this development were detected up to 140 m upstream of the

243 knickpoint (CS 512 m) in the transition section (CS 650 m – CS 550 m; Fig. 1), defined (i) by a much bigger flow competence

244 (largest particle a flow can move) than in the headwater and (ii) the exposure of already very big non-fluvial sediments (*b*>

245 2000 mm). Similar to the canyon, fine fractions are expected to be transported continuously out of the headwater, which will

246 result in progressive armoring of the channel bed by sediment coarsening (Bunte & Abt, 2001; Dietrich et al., 1989). Exactly

247 this post-glacial fluvial development is already occurring in the steep canyon. The local sorting of the diamicton by glacifluvial

248 erosion resulted in channel bed incision (Fig. 6). The calculation results, according to the approach with I_{red} (Rickenmann et

249 al., 2006), valid for torrential flow characteristics (e.g., Pralong et al., 2015; Nitsche et al., 2011), indicate armor layer

250 formation in the entire canyon. Due to decreasing flow competence by changing hydrology in the long-term perspective (e.g.,

251 Huss & Hock, 2018; Förster et al., 2015; Schöner et al., 2013; Haeberli et al., 2011), the channel bed of the already incised

252 canyon will stabilize at d_{50}= 600 mm from a hydraulic point of view (Fig. 3b). Less bedload transport at the foreland of the

253 Pasterze was already observed by Avian et al. (2018) and Geilhausen et al. (2012b).

254 The progressive armoring by (i) glacifluvial erosion combined with (ii) decreasing flow competence in the long-term

255 perspective (Pralong et al., 2015) will establish an erosion-resistant pavement layer. In contrast to the infrequently mobile

256 armoring layer (Bunte & Abt, 2001), this development will prevent channel bed incision by exposing non-fluvial deposits of

257 the diamictic glacier foreland (outwash plain). The beginning of this trend was already observed in characteristic points in the

258 canyon (triangles in Fig. 1), where very coarse (non-fluvial) sediment composition was occasionally measurable (up to d_{90}=

259 850 mm; Fig. 3). These points indicate the assumption of limited channel bed incision in the future and are labeled 'erosion

260 breakpoints' (Fig. 6). For rivers characterized by such post-glacial non-fluvial sediment, Hauer & Pulg (2018) implemented

261 the term glacial-till cascade, which contributes remarkably to channel stabilization.
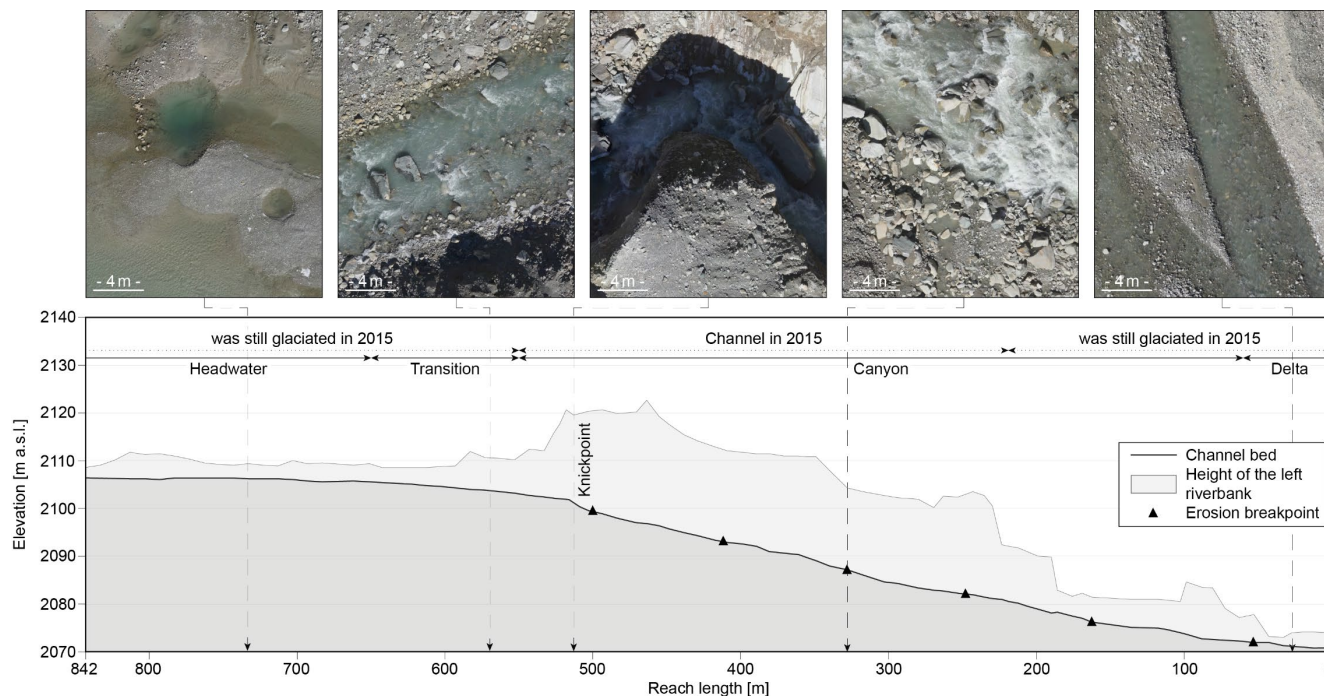
Figure 6: Longitudinal section of the investigated reach length with (i) the upper edge of the riverbank and (ii) predicted 'erosion breakpoints' according to the study results. The information about the glacierized area in 2015 originated from the orthophoto of 2015 (compare Fig. 5). In addition, pictures taken during UAV mapping show the sediment composition in some characteristic points.

The gradual evolution of proglacial channels in diamictic glacifluvial deposits starts as braided channels in direct glacier proximity (e.g., Marren, 2005; Gurnell et al., 1999). According to this development, glacifluvial erosion, predominant for sediment reworking (Church & Ryder, 1972), is defined in a generalized way as the last transport process of the proglacial sediment cascade model (Geilhausen et al., 2012b). However, according to the predicted study results, limited flow competence by 2050 (also compare Pralong et al., 2015) will develop a new in-stream storage type within the fluvial system of the sediment cascade model, defined by the erosion-resistant pavement layer (grey highlighted in Fig. 7). This extension by the new in-stream storage type (non-fluvial deposit) is accompanied by the refinement of the fluvial system within subsystem IV of the sediment cascade approach (dotted frames in Fig. 7). Glacifluvial erosion and the exposure of non-fluvial sediment lead inventible to a needed differentiation of the transport limited braided channel in direct glacier proximity and the (partly) supply limited 'developed channel' with a greater distance to the glacier terminus. Furthermore, established pavement layers disconnect the linkage between the proglacial channel bed and the unconsolidated diamictic sediment in the subsurface (e.g., Fryris et al., 2007; Brierley et al., 2006).
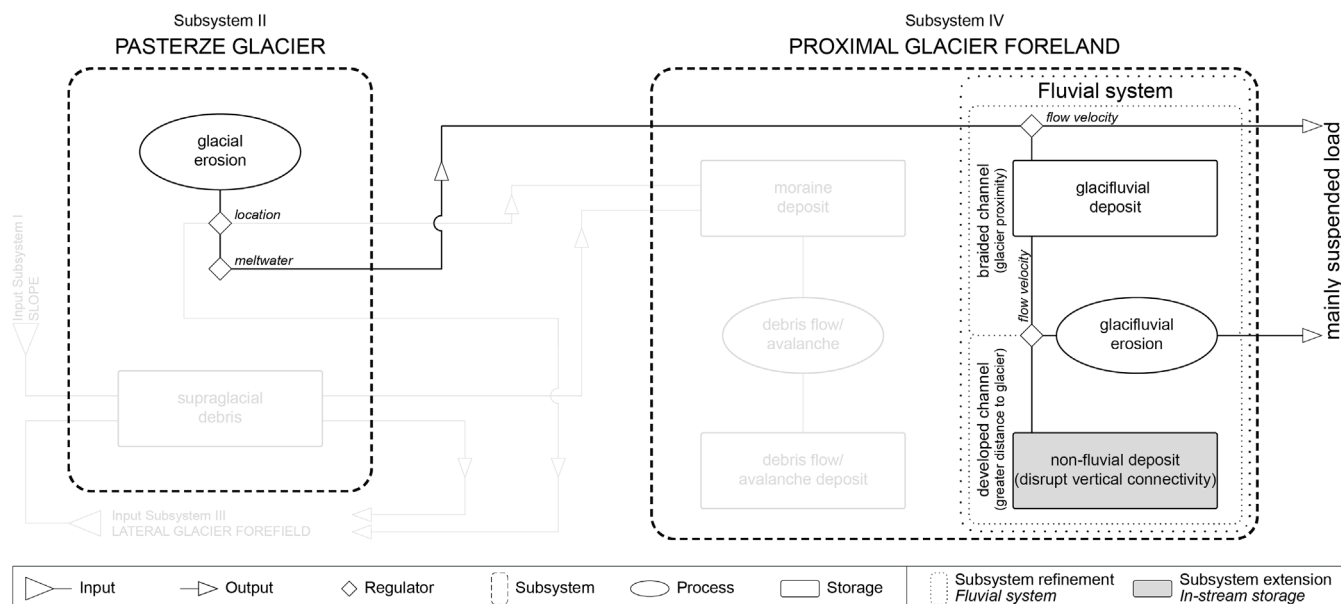
Figure 7: Refinement (dotted frames) and extension (grey highlighted in-stream sediment storage type) by the fluvial system within subsystem IV (proximal glacier foreland) of the conceptual model of a sediment cascade for proglacial catchments. The establishment of a pavement layer by non-fluvial deposits will disrupt the vertical connectivity between the proglacial channel bed and the subsurface. Due to the decoupled subsystems in the catchment (Geilhausen et al., 2012b), the grey-coloured connections only complete the cascade model but are irrelevant to the objectives of this study. Modified after Geilhausen et al. (2012b).

Pavement layer formation by glacifluvial erosion is thus an essential stabilization as part of the well-known landform decoupling (e.g., Bakker et al., 2018; Wohl et al., 2015; Fryris et al., 2007) or (ii) vegetation cover within a river system (e.g., Eichel et al., 2018; Klaar et al., 2015; Gurnell et al., 1999). As the sediment cascade model shows decoupled subsystems in the Pasterze catchment (Geilhausen et al., 2012b), the new in-stream storage type is composed of non-fluvial glacial deposits. In order that the subsystems of a sediment cascade model are coupled with each other, coarse colluvial deposits can also be contained in this non-fluvial sediment storage type and contribute to channel stabilization (Carrivick & Rushmer, 2009). These developed channels will prevent further channel bed incision but will still allow lateral sediment supply, often triggered by high-magnitude/low-frequency events (e.g., Baewert & Morche, 2014; Marren, 2005; Old et al., 2005; Beylich & Gintz, 2004). Measurements in high mountain areas are prone to uncertainties, as (i) inaccessibility and (ii) torrential flow characteristics lead to limitations in the (i) geometry and calibration data acquisition as well as in sediment sampling. Due to low flow conditions during the in-situ measurements, representative sediment analysis of the canyon could be done in the partly wetted area. It is assumed that the same grain size composition is present in the permanently wetted area, although it will probably be already coarser due to constant exposition to glacifluvial erosive processes. However, the applied method of investigating the sediment composition (photogrammetrically in the inaccessible canyon) is satisfactory, as all grain sizes smaller than the lower threshold ($b > 65$ mm) are irrelevant for the pavement layer formation. Furthermore, simplifications were applied to the calculation approach (e.g., neglect of near-bed turbulence).

5.2 Drivers for future proglacial channel avulsion

Glacifluvial sediment reworking of glacial deposits reduces landform connectivity and leads to a progressive stabilizing of proglacial areas (Lane et al., 2016). Connectivity in turn is crucial for sediment storage or export (Bakker et al., 2018; Geilhausen et al., 2012b). While proglacial lakes, like the 'Sandersee' or 'Pasterzensee' (Fig. 1), act as sediment traps (e.g., Bogen et al., 2014; Geilhausen et al., 2013; Krainer & Poscher 1992), the melt-out of (buried) dead ice landforms are still a hidden effect on proglacial channel evolution, especially in recently deglaciated areas (e.g., Avian et al., 2018; Delaney et al., 2018; Lane et al., 2016). In contrast to flood-driven river avulsion (e.g., Slingerland & Smith, 2004; Jones & Schumm, 1999; Brizga & Finlayson, 1990), proglacial channel avulsion may be caused by the downwasting of dead ice landforms (e.g., Benn & Evans, 2013; Lukas, 2011; Bennett and Glasser, 2009; Lukas et al., 2005; Richardson & Reynolds, 2000). Furthermore, the melt-out of buried dead ice beyond the channel in the subsurface can result in channel bed settlement. However, this process will not change the sediment composition of the erosion-resistant pavement layer of non-fluvial sediment. One prerequisite for the development of such landforms is debris-covered glacier surface (Benn & Evans, 2013), whose progressive increase can be observed worldwide (Mayr & Haag, 2019), in Europe (Lardeux et al., 2016), and thus also at the glacier Pasterze (Fischer et al., 2018). Consequently, different dead ice landforms like hummocky moraines, ice-cored moraines, or kettles could be detected at the foreland of glacier Pasterze (e.g., Avian et al., 2018; Geilhausen et al., 2012b; Krainer & Poscher, 1992). Investigating channel evolution in response to melting dead ice landforms is highly relevant to (i) describing future proglacial channel development and (ii) quantifying proglacial sediment yields and sediment dynamics.

6 Summary and Conclusion

The distinction and transition from armor layers to erosion-resistant pavement layers by non-fluvial sediment is an important definition and process in the proglacial channel evolution. Triggered by runoff variability due to global warming, the establishment of non-erodible pavement layers is an essential post-glacial development process and has been widely neglected up to now in defining proglacial channel evolution stages.

(1)   While recently deglaciated river sections are prone to glacifluvial headward erosion (against flow direction parallel to glacier retreat) due to the fine sediment composition of the outwash plain, river sections with a greater distance to the glacier terminus are characterized by sediment coarsening. This gradual process will limit further channel bed incision by establishing an erosion-resistant pavement layer by non-fluvial deposit. Triggered by global warming, the short-term increase and long-term decrease of the flow competence will develop pavement layers, which are in contrast to infrequently mobile armoring layers. This development is considered as a final process in proglacial river evolution.

(2)   The calculation results of non-fluvial deposits forming pavement layers allow the extension of the proglacial sediment cascade model by a new in-stream storage type within the fluvial system. This extension results in a refinement of the existing fluvial part of the cascade approach: (i) braided channels in direct glacier proximity differ from (ii) the 'developed

331   channels' with increasing distance to the glacier terminus. This development leads to vertical landform decoupling
332   between the erosion-resistant proglacial channel bed and the unconsolidated diamictic sediment in the subsurface.

333   (3)   In the long-term perspective, river avulsion driven by the melt-out of (buried) dead ice landforms will mainly contribute
334   to the stabilization in the catchment and reach scale. Investigating the channel evolution in response to melting dead ice
335   landforms is highly relevant for quantifying future post-glacial sediment dynamics. However, due to the characteristics
336   of glacial diamicton (poorly sorted sediment matrix ranging in size from sand up to boulders), proglacial channel
337   evolution will always lead to the final stage of pavement layer formation, as proven and described in this study.

Data availability

339   All the experimental data used in this study are available from the authors upon request.

Author contribution

341   MP and CH planned and designed the research. MP, PF, AN, GW, and BH performed the investigation, data curation, and
342   evaluation. The original draft preparation and visualization were done by MP and CH with equal contributions from all co-
343   authors. All authors were part of the review and editing of the manuscript.

Competing interests

345   The authors declare that they have no conflict of interest.

Disclaimer

347   Publisher's note: Copernicus Publications remains neutral with regard to jurisdictional claims in published maps and
348   institutional affiliations.

Acknowledgment

Hydrology and
Earth System
Sciences
Discussions

References

355

356 Alley, R.B., Cuffey, K.M., Zoet, L.K.: Glacial erosion: status and outlook, Annals of Geology, 60, 1–13, doi:
357   10.1017/aog.2019.38, 2019.

358 Ashworth, P.J., Ferguson, R.I.: Interrelationships of Channel Processes, Changes and Sediments in a Proglacial Braided River,
359   Geogr. Ann. A., 68, 361–371, doi:10.1080/04353676.1986.11880186, 1986.

360 Avian, M., Bauer, C., Schlögl, M., Widhalm, B., Gutjahr, K.-H., Paster, M., Hauer, C., Frießenbichler, M., Neureiter, A.,
361   Weyss, G., Flödl, P., Seier, G., Sulzer, G.: The Status of Earth Observation Techniques in Monitoring High Mountain
362   Environments at the Example of Pasterze Glacier, Austria: Data, Methods, Accuracies, Processes, and Scales, Remote
363   Sens., 12, 1251, doi:10.3390/rs12081251, 2020.

364 Baewert, H., Morche D.: Coarse sediment dynamics in a proglacial fluvial system (Fagge River, Tyrol), Geomorphology, 218,
365   88–97, doi:10.1016/j.geomorph.2013.10.021, 2014.

366 Bakker, M., Costa, A., Silva, T.A., Stutenbecker, L., Girardclos, S., Loizeau, J.-L., Molnar, P., Schlunegger, F., Lane, S.N.:
367   Combined Flow Abstraction and Climate Change Impacts on an Aggrading Alpine River, Water Resour. Res., 54, 223 –
368   242, doi:10.1002/2017WR021775, 2018.

369 Ballantyne, C.K.: Paraglacial geomorphology, Quaternary Sci. Rev., 21, 1935–2017, doi:10.1016/S0277-3791(02)00005-7,
370   2002.

371 Benn, D.I., Evans, D.J.A.: Glaciers & Glaciation, Routledge, London, UK, 2013.

372 Bennett, M., Glasser, N.F.: Glacial Geology: Ice sheets and landforms, Chichester, UK; Hoboken, NJ: Wiley-Blackwell, 2009.

373 Beylich, A., Gintz, D.: Effects of High-Magnitude/Low-Frequency Fluvial Events Generated by Intense Snowmelt or Heavy
374   Rainfall in Arctic Periglacial Environments in Northern Swedish Lapland and Northern Siberia, Geogr. Ann. A., 86, 11–
375   29, doi:10.1111/j.0435-3676.2004.00210.x, 2004.

376 Beylich, A., Laute, K., Liermann, S., Hansen, L., Burki, V., Vatne, G., Fredin, O., Gintz, D., Berthling, I.: Subrecent sediment
377   dynamics and sediment budget of the braided sandur system at Sandane, Erdalen (Nordfjord, Western Norway), Norwegian
378   Journal of Geography, 63: 123–131, doi:10.1080/00291950902907934, 2009.

379 Bogen, J., Xu, M., Kennie, P.: The impact of proglacial lakes on downstream sediment delivery in Norway. Earth Surf. Proc.
380   and Land., 40, 942–952, doi:10.1002/esp.3669, 2014.

381 Braun, L.N., Weber, M., Schulz, M.: Consequences of climate change for runoff from Alpine regions, Ann. Glaciol., 31: 19–
382   25, doi:10.3189/172756400781820165, 2000.

383 Brierley, G., Fryirs, K., Jain, V.: Landscape connectivity: the geographic basis of geomorphic applications, Area, 38, 165–
384   174, doi:10.1111/j.1475-4762.2006.00671.x, 2006.

385 Brizga, S.O., Finlayson, B.L.: 1990. Channel avulsion and river metamorphosis: The case of the Thomson River, Victoria,
386   Australia, Earth Surf. Proc. and Land., 15, 391–404, doi:10.1002/esp.3290150503, 1990.

387 Bunte, K., Abt, S.R.: Sampling surface and subsurface particle-size distributions in wadable gravel-and cobble-bed streams
388   for analyses in sediment transport, hydraulics, and streambed monitoring, Gen. Tech. Rep. RMRS-GTR-74, Fort Collins,
389   CO: U.S. Department of Agriculture, Forest Service, Rocky Mountain Research Station, 2001.

390 Carrivick, J.L., Geilhausen, M., Warburton, J., Dickson, N.E., Carver, S.J., Evans, A.J., Brown, L.E.: Contemporary
391   geomorphological activity throughout the proglacial area of an alpine catchment, Geomorphology, 188, 83–95,
392   doi:10.1016/j.geomorph.2012.03.029, 2013.

393   Carrivick, J.L., Rushmer, E.L.: Inter- and Intra-catchment Variations in Proglacial Geomorphology: An Example from Franz
394   Josef Glacier and Fox Glacier, New Zealand, Arctic, Antarctic, and Alpine Research, 41, 18-36, doi:10.1657/1523-0430-
395   41.1.18, 2009.

396   Cavalli, M., Trevisani, S., Comiti, F., Marchi, L.: Geomorphometric assessment of spatial sediment connectivity in small
397   Alpine catchments, Geomorphology, 188: 31–41, doi:10.1007/978-3-319-94184-4_16, 2013.

398   Chorley, R.J., Kennedy, B.A.: Physical geography: a system approach, Prentice-Hall, London, UK, 1971.

399   Church, M., Ryder, J.M.: Paraglacial Sedimentation: A Consideration of Fluvial Processes Conditioned by Glaciation, GSA
400   Bulletin, 83, 3059–3072, doi:10.1130/0016-7606(1972)83[3059:PSACOF]2.0.CO;2, 1972.

401   Delaney, I., Bauder, A., Huss, M., Weidmann, Y.: Proglacial erosion rates and processes in a glacierized catchment in the
402   Swiss Alps, Earth Surf. Proc. and Land., 43, 765–778, doi:10.1002/esp.4239, 2018.

403   Detert, M., Kadinski, L., Weitbrecht, V.: On the way to airborne gravelometry based on 3D spatial data derived from images,
404   Int. J. Sediment Res., 33, 84–92, doi: 10.1016/j.ijsrc.2018.02.001, 2018.

405   Dietrich, W.E., Kirchner, J.W., Ikeda, H., Iseya, F.: Sediment supply and the development of the coarse surface layer in gravel-
406   bedded rivers, Nature, 340: 215 –217, doi:10.1038/340215a0, 1989.

407   Eichel, J., Draebing, D., Meyer, N.: From active to stable: Paraglacial transition of Alpine lateral moraine slopes, Land Degrad.
408   Dev., 29, 4158–4172, doi:10.1002/ldr.3140, 2019.

409   Etzelmüller, B., Frauenfelder, R.: Factors Controlling The Distribution of Mountain Permafrost in The Northern Hemisphere
410   and Their Influence on Sediment Transfer, Arctic, Antarctic, and Alpine Research, 41, 48–58, doi:10.1657/1523-0430-
411   41.1.48, 2009.

412   Farinotti, D., Usselmann, S., Huss, M., Bauder, A., Funk, M.: Runoff evolution in the Swiss Alps: projections for selected
413   high-alpine catchments based on ENSEMBLES scenarios, Hydrol. Process., 26: 1909–1924, doi:10.1002/hyp.8276, 2012.

414   Fehr R.: Einfache Bestimmung der Korngrössenverteilung von Geschiebematerial mit Hilfe der Linienzahlanalyse, Schweizer
415   Ingenieur Und Architekt, 105, 1104–1009, doi:10.5169/seals-76710, 1987, [in german].

416   Fischer, A., Patzelt, G., Achrainer, M., Groß, G., Lieb, G. K., Kellerer-Pirklbauer, A., Bendler, G.: Gletscher im Wandel: 125
417   Jahre Gletschermessdienst des Alpenvereins, Berlin, Germany: Springer Spektrum, 2018, [in german].

418   Fonstad, M.A., Dietrich, J.T., Courville, B.C., Jensen, J.L., Carbonneau, P.E.: Topographic Structure from Motion: A New
419   Development in Photogrammetric Measurement, Earth Surf. Proc. and Land., 38, 421–430, doi:10.1002/esp.3366, 2013.

420   Förster, K., Oesterle, F., Hanzer, F., Huttenlau, M., Strasser, U.: Bestimmung der Auswirkungen des Klimawandels auf die
421   Gletscherdynamik und das Abflussregime im Rofental unter Verwendung eines gekoppelten glazio-hydrologischen
422   Modells. In Institut für Geographie der Universität Innsbruck [Ed]. Innsbrucker Jahresberichte 2014-2015: 23–40,
423   Innsbruck, Austria: Institut für Geographie der Universität Innsbruck, 2015, [in german].

424   Fryris, K., Brierley, G., Preston, N., Kasai, N.: Buffers, barriers and blankets: The (dis)connectivity of catchment-scale
425   sediment cascades, CATENA, 70: 49–67, doi: 10.1016/j.catena.2006.07.007, 2007.

426   Geilhausen, M., Otto, J-C., Morche, D., Schrott, L.: Decadal sediment yield from an Alpine proglacial zone inferred from
427   reservoir sedimentation (Pasterze, Hohe Tauern, Austria), IAHS Publication, 356: 161–172, 2012a.

428   Geilhausen, M., Otto, J-C., Schrott, L.: Spatial distribution of sediment storage types in two glacier landsystems (Pasterze &
429   Obersulzbachkees, Hohe Tauern, Austria), J. Maps, 8, 242–259, doi:10.1080/17445647.2012.708540, 2012b.

430   Geilhausen, M., Morche, D., Otto, J.-C., Schrott, L.: Sediment discharge from the proglacial zone of a retreating Alpine glacier,
431   Z. Geomorphol., 57, 29 –53, doi:10.1127/0372-8854/2012/S-00122, 2013.

432 Gruber, S., Hoelzle, M., Haeberli, W.: Permafrost thaw and destabilization of Alpine rock walls in the hot summer of 2003,
433   Geophys. Res. Lett., 31, doi:10.1029/2004GL020051, 2004.

434 Gurnell, A.M., Edwards, P.J., Petts, G.E., Ward J.V.: A conceptual model for alpine proglacial river channel evolution under
435   changing climatic conditions, CATENA, 38, 223–242, doi:10.1016/S0341-8162(99)00069-7, 1999.

436 Haeberli, W., Job, D., Boogen, N., Raymond Pralong, M., Schneider, R., Dupraz, C., Glassey, T., Rietmann, D., Usselmann,
437   S., Ewen, T., Bobierska, F., Metraux, V., Beer, A., Hänggi, P., Stähli, M., Bosshard, T., Turowski, J., Ludwig ,A., Paul,
438   F., Farinotti, D., Rickenmann, D., Mueller, C., Bauder, A., Helland, E., Widmer, .F., Ossiaa, M., Fankhauser, A., Zappa,
439   M., Jonas, T., Linsbauer, A., Spreng, D., Schär, C., Weingartner, R., Angehrn, S., Kotlarski, S.: Auswirkungen der
440   Klimaänderung auf die Wasserkraftnutzung: Synthesebericht. Schweizerische Gesellschaft für Hydrologie und Limnologie
441   (SGHL), Hydrologische Kommission (CHy) [Eds], Beiträge zur Hydrologie der Schweiz, 2011, [in german].

442 Harland, W.B., Herod, K.N., Krinsley, D.H.: The definition and identification of tills and tillites, Earth-Sci. Rev., 2, 225–256,
443   doi:10.1016/0012-8252(66)90030-4, 1966.

444 Harris, C., Arenson, L., Etzelmüller, B., Frauenfelder, F., Gruber, S., Haeberli, W., Hauck, C., Hölzle, M., Humlum, O.,
445   Isaksen, L., Kääb, A., Kern-Lütschg, M.A., Lehning, M., Matsuoka, N., Murton, J.B., Nötzli, J., Philips, M., Ross, N.,
446   Seppälä, M, Springman, S.M., Vonder Mühll, D.: Permafrost and climate in Europe: Monitoring and modelling thermal,
447   geomorphological and geotechnical responses, Earth-Sci. Rev., 92, 117–171, doi:10.1016/j.earscirev.2008.12.002, 2009.

448 Hauer, C., Pulg U.: The non-fluvial nature of Western Norwegian rivers and the implications for channel patterns and sediment
449   composition, CATENA, 171: 83–98, doi:10.1016/j.catena.2018.06.025, 2018.

450 Heckmann, T., Morche, D.: Geomorphology of Proglacial Systems: Landform and Sediment Dynamics in Recently
451   Deglaciated Alpine Landscapes, Geography of the Physical Environment, Springer, Cham, 2019

452 Hilgendorf, Z., Wells, G., Larson, P.H., Millet, J., Kohout M.: From basins to rivers: Understanding the revitalization and
453   significance of top-down drainage integration mechanisms in drainage basin evolution. Geomorphology, 352, 107020.
454   doi:10.1016/j.geomorph.2019.107020, 2020.

455 Huss, M. Hock, R.: Global-scale hydrological response to future glacier mass loss, Nature Clim. Change, 8, 135–140,
456   doi:10.1038/s41558-017-0049-x, 2018.

457 Huss, M., Farinotti, D., Bauder, A., Funk, M.: Modelling runoff from highly glacierized alpine drainage basins in a changing
458   climate, Hydrol. Process., 22, 3888–3902, doi:10.1002/hyp.7055, 2008.

459 Jones, L.S., Schumm, S.A.: Causes of Avulsion: An Overview. In Smith, N.D., Rogers, J. [Eds], Fluvial Sedimentology VI,
460   169 – 178, Hoboken, NJ: Wiley-Blackwell, 1999.

461 Kellerer-Pirklbauer, A.: The Supraglacial Debris System at the Pasterze Glacier, Austria: Spatial Distribution, Characteristics
462   and Transport of Debris, Z. Geomorphol. Supp., 52, 3–25, doi: 10.1127/0372-8854/2008/0052S1-0003, 2008.

463 Kellerer-Pirklbauer, A., Lieb, G.K., Avian, M., Gschpurning, J.: The response of partially debris-covered valley glaciers to
464   Climate Change: The example of the Pasterze glacier (Austria) in the period 1964 to 2006, Geogr. Ann. A., Physical
465   Geography, 90, 269–285, doi:10.1111/j.1468-0459.2008.00345.x, 2008.

466 Klaar, M.J., Kidd, C., Edward, M., Rebecca, B., Gilles, P., Chapin, F.S., Milner, A.: Vegetation succession in deglaciated
467   landscapes: implications for sediment and landscape stability, Earth Surf. Proc. and Land., 40 (88), 1088–1100,
468   doi:10.1002/esp.3691, 2015.

469 Krainer, K. & Poscher, G.: Sedimentologische Beobachtungen am Gletschervorfeld der Pasterze (Glocknergruppe, Hohe
470   Tauern), Carinthia II, 182 (102), 317–343, 1992, [in german].

471 Lane, S.N., Bakker, M., Gabbud, C., Micheletti, N., Saugy, J.-N.: Sediment export, transient landscape response and
472   catchment-scale connectivity following rapid climate warming and Alpine glacier recession, Geomorphology, 277, 210–
473   227, doi:10.1016/j.geomorph.2016.02.015, 2016.

474 Lang, N., Irniger, A., Rozniak, A., Hunziker, R., Wegner, J.D., Schindler, K.: GRAINet: mapping grain size distributions in
475   river beds from UAV images with convolutional neural networks, Hydrol. Earth Syst. Sc., 25, 2567–2597, doi:
476   10.5194/hess-25-2567-2021, 2021.

477 Lardeux, P., Glasser, N., Holt, T., Hubbard, B.: Debris-covered glaciers extend the lifespan of water supplies in the European
478   Alps, EGU General Assembly, 18, 2016.

479 Leggat, M.S., Owens, P.N., Stott, T.A., Forrester, B.J., Déry, S.J., Menounos, B.: Hydro-meteorological drivers and sources
480   of suspended sediment flux in the pro-glacial zone of the retreating Castle Creek Glacier, Cariboo Mountains, British
481   Columbia, Canada, Earth Surf. Proc. and Land., 40, 1542–1559, doi:10.1002/esp.3755, 2015.

482 Lukas, S.: Ice-Cored Moraines. In: Encyclopedia of Snow, Ice and Glaciers. Singh, V.P., Singh, P., Haritashya, U.K. [Eds],
483   Dordrecht, Springer Netherlands, doi:10.1007/978-90-481-2642-2_666, 2011.

484 Lukas, S., Nicholson, L.I., Ross, F.H., Humlum, O.: Formation, Meltout Processes and Landscape Alteration of High-Arctic
485   Ice-Cored Moraines – Examples From Nordenskiold Land, Central Spitsbergen, Polar Geography, 29, 157–187,
486   doi:10.1080/789610198, 2005.

487 Maizels, J.K.: Sediments and landforms of modern proglacial terrestrial environments. In: Menzies, J. [Ed], Modern Glacial
488   Environments, Butterworth-Heinemann, Oxford, 2002.

489 Mao, L., Dell'Agnese, A., Huincache, C., Penna, D., Engel, M., Niedrist, G., Comiti, F.: Bedload hysteresis in a glacier-fed
490   mountain river, Earth Surf. Proc. and Land., 39, 964–976, doi:10.1002/esp.3563, 2014.

491 Marren, P.M.: Magnitude and frequency in proglacial rivers: a geomorphological and sedimentological perspective, Earth-Sci.
492   Rev., 70, 203–251, doi:10.1016/j.earscirev.2004.12.002, 2005.

493 Mayr, E., Hagg, W.: Debris-Covered Glaciers. In: Heckmann, T. & Morche, D. [Eds.]: Geomorphology of Proglacial Systems,
494   59 –71, 2019.

495 Micheletti, N., Lambiel, C., Lane, S.: Investigating decadal-scale geomorphic dynamics in an alpine mountain setting, J.
496   Geophys. Res.-Earth., 120, 2155–2175, doi:10.1002/2015JF003656, 2015.

497 Nitsche, M., Rickenmann, D., Turowski, J.M., Badoux, A.: Evaluation of bedload transport predictions using flow resistance
498   equations to account for macro-roughness in steep mountain streams, Water Resour. Res., 47, W08513,
499   doi:10.1029/2011WR010645, 2011.

500 Old, G.H., Lawler, D.M., Snorrason A.: Discharge and suspended sediment dynamics during two jökulhlaups in the Skaftá
501   river, Iceland. Earth Surf. Proc. and Land., 30, 1441–1460, doi:10.1002/esp.1216, 2005.

502 Pralong, R.M., Turowski, J.M., Rickenmann, D., Turowski, J.M., Rickenmann, D., Zappa, M.: Climate change impacts on
503   bedload transport in alpine drainage basins with hydropower exploitation, Earth Surf. Proc. and Land., 40, 1587–1599,
504   doi:10.1002/esp.3737, 2015.

505 Richardson, S.D., Reynolds, J.M.: Degradation of ice-cored moraine dams: implications for hazard development. Proceeding
506   Workshop Seattle, Washington, 264, 187–197, 2000.

507 Rickenmann, D.: Bedload Transport Capacity of Slurry Flows at Steep Slopes, Mitteilungen der Versuchsanstalt für
508   Wasserbau, Hydrologie und Glaziologie der Eidgenössischen Technischen Hochschule Zürich, 103: 8–249, 1990.

509 Rickenmann, D., Chiari, M., Friedl, K.: SETRAC – A sediment routing model for steep torrent channels. In: Ferreira, R.M.L.,
510   Alves, E., Leal, J., Cardoso, A. [Eds], River Flow 2006, proceedings of the International Conference on Fluvial Hydraulics,
511   Lisbon, Portugal, 6-8 September 2006, London, Taylor & Francis, doi:10.1201/9781439833865.ch88

512 Schaefli, B.: Projecting hydropower production under future climates: a guide for decision-makers and modelers to interpret
513   and design climate change impact assessments, Wiley Interdisciplinary Reviews: Water, 2, 271–289,
514   doi:10.1002/wat2.1083, 2015.

515 Schlunegger, F., Schneider H.: Relief-rejuvenation and topographic length scales in a fluvial drainage basin, Napf area, Central
516   Switzerland, Geomorphology, 69, 102–117, https://doi.org/10.1016/j.geomorph.2004.12.008, 2005.

517 Schöner, W., Reisenhofer, S., Neureiter, A.: EURAS-CLIMPACT Impact of climate change and related glacier hazards and
518   mitigation strategies in the European Alps, Swedish Lapland and the Tien Shan Mountains, Central Asia, Vienna, Austria,
519   Zentralanstalt für Meteorologie und Geodynamik, 2013.

520 Schrott, L., Hufschmidt, G., Hankammer, M., Hoffmann, T., Dikau, R.: Spatial distribution of sediment storage types and
521   quantification of valley fill deposits in an alpine basin, Rheintal, Bavarian Alps, Germany, Geomorphology, 55, 45–63,
522   doi:10.1016/S0169-555X(03)00131-4, 2003.

523 Slaymaker, O.: Proglacial, periglacial or paraglacial?, Geol. Soc. Sepc. Publ., 320, 71–84, https://doi.org/10.1016/S0169-
524   555X(03)00131-4, 2009.

525 Slingerland, R., Smith, N.: River avulsion and deposition, Annu. Rev. Earth Pl. Sc., 32, 257–285. doi:
526   10.1146/annurev.earth.32.101802.120201, 2004

527 Snavely, N., Seit, S.M., Szeliski, R.: Modeling the world from internet photo collections, Int. J. Comput. Vision, 80, 189–210,
528   doi:10.1007/s11263-007-0107-3, 2008.

529 Sommer, C., Malz, P., Seehaus, T.C., Lippl, S., Zemp, M., Braun, M.H.: Rapid glacier retreat and downwasting throughout
530   the European Alps in the early 21st century, Nature Commun., 11, 3209, doi:10.1038/s41467-020-16818-0, 2020.

531 Wilkie, K., Clague, J.J.: Fluvial response to Holocene glacier fluctuations in the Nostetuko River valley, southern Coast
532   Mountains, British Columbia, Geological Society, 320, 199–218, doi:10.1144/SP320.13, 2009.

533 Wohl, E., Bledsoe, B.P., Jacobsen, R.B., Poff, N.L., Rathburn, S.L., Walters, D.M., Wilcox, A.C.: The Natural Sediment
534   Regime in Rivers: Broadening the Foundation for Ecosystem Management, BioScienc, 65, 358–371. doi:
535   10.1093/biosci/biv002, 2015

536 Zemp, M., Huss, M., Thibert, E., Eckert, N., McNabb, R., Huber, J., Barandun, M., Machguth, H., Nussbaumer, S.U., Gärtner-
537   Roer, I., Thomson, L., Paul, F., Maussion, F., Kutuzov, S., Cogley, J.G.: Global glacier mass changes and their
538   contributions to sea-level rise from 1961 to 2016, Nature, 568, 382–386, doi:10.1038/s41586-019-1071-0, 2019.